Mechanisms linking active rock glaciers and impounded surface water formation in high-mountain areas

Mechanisms linking active rock glaciers and impounded surface water formation in high-mountain areas

Corresponding Author: Nicola Colombo

University of Turin Department of Earth Sciences Via Valperga Caluso 35 Turin Piemonte Italy 10125

Carleton University Department of Geography and Environmental Studies Loeb Building, 1125 Colonel By Drive Ottawa Ontario Canada K1S 5B6

Email Add: nicola.colombo@unito.it

http://orcid.org/0000-0003-2244-3147

Author: Luigi Sambuelli

Polytechnic University of TurinDepartment of Environment, Land and Infrastructure Engineering

Corso Duca degli Abruzzi 24 Turin Italy 10129

Email Add: luigi.sambuelli@polito.it

Author: Cesare Comina

University of Turin Department of Earth Sciences Via Valperga Caluso 35 Turin Italy 10125

Email Add: cesare.comina@unito.it

Author: Chiara Colombero

University of Turin Department of Earth Sciences Via Valperga Caluso 35 Turin Italy 10125

Email Add: chiara.colombero@unito.it

Author: Marco Giardino

University of Turin Department of Earth Sciences Via Valperga Caluso 35 Turin Italy 10125

Email Add: marco.giardino@unito.it

Author: Stephan Gruber

Carleton University Department of Geography and Environmental Studies Loeb Building, 1125 Colonel By Drive Ottawa Ontario Canada K1S 5B6

Email Add: stephan.gruber@carleton.ca

This article has been accepted for publication and undergone full peer review but has not been through the copyediting, typesetting, pagination and proofreading process which may lead to differences between this version and the Version of Record. Please cite this article as doi: 10.1002/esp.4257

Author: Gaetano Viviano

CNR - National Research Council IRSA - Water Research Institute Via del Mulino 19 Brugherio Italy 20047

Email Add: viviano@irsa.cnr.it

Author: Livia Vittori Antisari

University of Bologna Department of Agricultural Sciences Viale Fanin 40 Bologna Italy 40127

Email Add: livia.vittori@unibo.it

Author: Franco Salerno

CNR - National Research Council IRSA - Water Research Institute Via del Mulino 19 Brugherio Italy 20047

Author: salerno@irsa.cnr.it

ABSTRACT

Rock glaciers are slowly flowing mixtures of debris and ice occurring in mountains. They can represent a reservoir of water, and melting ice inside them can affect surface water hydrochemistry. Investigating the interactions between rock glaciers and water bodies is therefore necessary to better understand these mechanisms. With this goal, we elucidate the hydrology and structural setting of a rock glacier-marginal pond system, providing new insights into the mechanisms linking active rock glaciers and impounded surface waters. This was achieved through the integration of waterborne geophysical techniques (ground penetrating radar, electrical resistivity tomography and self-potentials) and heat tracing. Results of these surveys showed that rock glacier advance has progressively filled the valley depression where the pond is located, creating a dam that could have modified the level of impounded water. A sub-surface hydrological window connecting the rock glacier to the pond was also detected, where an inflow of cold and mineralised underground waters from the rock glacier was observed. Here, greater water contribution from the rock glacier occurred following intense precipitation events during the ice-free season, with concomitant increasing electrical conductivity values. The outflowing dynamic of the pond is dominated by a sub-surface seepage where a minor fault zone in bedrock was found, characterised by altered and highly-fractured rocks. The applied approach is evaluated here as a suitable technique for investigating logistically-complex hydrological settings which could be possibly transferred to wider scales of investigation.

1. INTRODUCTION

Active rock glaciers are widespread in cold mountain regions and contain ice-rich permafrost. They are debris covered and slowly flowing mixtures of debris and ice which form by processes on a continuum from glacial to periglacial (for a review: Haeberli et al., 2006). Active rock glaciers can represent an important water source (e.g., Corte, 1976; Azócar and Brenning, 2010; Millar et al., 2013), especially in arid areas and during low-flow conditions (e.g., Brenning, 2005; Azócar and Brenning, 2010; Rangecroft et al., 2015). Their hydrological significance relates to the long-term storage of frozen water, the seasonal storage and release of water, and the interaction with water flowing through or beneath them (Burger et al., 1999).

Water draining from rock glaciers is usually released at springs near the front, mostly as single streams, and sometimes as groundwater (Berger et al., 2004). Discharge is usually characterised by strong diurnal and seasonal variations, with high peaks associated with snowmelt and rainfall (Krainer and Mostler, 2002). Even during strongly varying discharge, water draining from active rock glaciers has been reported to be around the freezing point (Krainer et al., 2007; Millar et al., 2013).

Rock glaciers and hydrologically connected lakes and ponds can create specific ecosystems sensitive to climate change. For example, increased electrical conductivity and metal concentrations in some lakes of the European Alps were attributed to changed solute release from rock glaciers in response to atmospheric warming (Thies et al., 2007; Ilyashuk et al., 2014). Other studies reported increased electrical conductivity from May to October in the outflow of rock glaciers (Krainer and Mostler, 2002; Krainer et al., 2007) due to increasing seasonal contributions of concentrated weathering fluxes from groundwater and icemelt (Williams et al., 2006).

Hydrological studies on rock glaciers are rare (e.g., Krainer and Mostler, 2002; Berger et al., 2004; Krainer et al., 2007). Indeed, the hydrology of rock glaciers is complicated because of unknown flow paths, phase change and an irregular distribution of frozen material (e.g., Burger et al., 1999). Moreover, hydrological research on outflows of active rock glaciers is difficult, because most water drains within the debris (Krainer and Mostler, 2002). The presence of multiple and often inaccessible springs can further increase uncertainties (Krainer et al., 2012) and where rock glaciers terminate in lakes or ponds discharge is difficult to measure.

In this context, waterborne geophysical methods can map hydrogeological information, correlating geophysical parameters to hydrological and geological properties (e.g., Befus et al., 2012; Colombero et al., 2014). Waterborne ground penetrating radar can be used for mapping bathymetry, deriving hypsographic curves, analysing bottom deposit characteristics, and investigating bottom strata (e.g., Lachhab et al., 2014; Sambuelli et al., 2015). Waterborne resistivity methods, such as electrical resistivity tomography with floating cables, can be also used to delineate groundwater-lake interactions (Befus et al., 2012), characterise lacustrine sediments (Rucker et al., 2011) and investigate the geological setting (Colombero et al., 2014). In shallow water, floating electrodes are preferable over bottom electrodes from a logistical point of view even though this causes a partial loss of resolution with depth (Loke and Lane, 2004). Moreover, combined acquisition of self-potential data can be used for determining upflow (positive anomalies) and downflow (negative anomalies) regions in subsurface flow (Ishido and Pritchett, 1999) and mapping groundwater-surface water exchange (Grangeia and Matias, 2012).

Although waterborne geophysical techniques allow definition of hydrogeological setting, they cannot discriminate among different water sources. The interactions

between surface and sub-surface waters are usually quantified through water balance investigations, although those alone cannot distinguish different sub-surface components (e.g., Siegel, 2008). Conversely, the use of tracers can be helpful in discriminating different contributions (e.g., Anderson, 2005; Langston et al., 2013). This includes the use of natural tracers such as heat, as well as artificially introduced chemical tracers. Artificial tracers can usually be used for short periods (e.g., Anderson, 2005) in remote and harsh environments. Conversely, heat can be used efficiently to determine groundwater seepage across streambeds (e.g., Schmidt et al., 2007; Constantz, 2008) and at the bottom of lakes (e.g., Langston et al., 2013). Waterborne geophysical techniques and natural tracers are rarely used in alpine headwater ponds (e.g., Langston et al., 2013) and their integration, despite great potential, remains untested in these environments to date.

The importance of rock glaciers in shaping high-elevation hydrological dynamics, specifically in affecting adjacent ponds, is barely known. Here, a local study in a pond that is in direct contact with a rock glacier is reported. The hydrological connections between the rock glacier and its marginal pond have been studied with waterborne ground penetrating radar, electrical resistivity tomography, self-potential measurements, and heat as a natural tracer. The research questions that motivated this study are: (i) How does the sub-surface structural setting of a rock glacier-pond system influence its geomorphological characteristics?; (ii) Which are the main processes driving the thermal and hydrological dynamics of a marginal rock glacier pond?; and (iii) Can waterborne geophysical techniques and their integration with non-invasive hydrological methods be considered powerful tools for investigating logistically complex high-elevation hydrological settings?

2. STUDY AREA

The Col d'Olen Rock Glacier Pond (45°52'8.22''N, 7°51'46.98''E, WGS84) is in the north-western Italian Alps (Fig. 1a and 1b) along the Aosta Valley and Piemonte Region border, at an elevation of 2722 m a.s.l. The catchment area is approximately 206,000 m^2 (Fig. 1c). The research site is a node of the Long-Term Ecological Research (LTER) network in Europe (http://www.lter-europe.net/). No studies have been previously carried out to investigate the periglacial and permafrost characteristics in this site.

The Col d'Olen area is dominated by glacial and periglacial features and it is situated on the southern slope of the Monte Rosa massif. It contains bedrock outcrops, and typical alpine deposits, landforms and habitat features that include talus slopes, snow beds, patterned ground and alpine meadows. Geologically, the study area is a significant tectonic intersection between major structural/paleogeographic domains of the Alpine orogen, with the presence (from North to South) of the Monte Rosa nappe, the "Zermatt-Saas" unit, the "Combin Zone" unit, and the Sesia Lanzo Zone (Dal Piaz, 2001; Handy et al., 2010; Gasco et al., 2011; Steck et al., 2015). In the Col d'Olen area, the tectonic contact between the "Zermatt Sass" unit (Corno Camoscio, 3024 m a.s.l.) and the overlaying "Combin Zone" unit is characterised by distinctive structural association of brittle faults and fractures whose main systems are approximately 110° and 60° oriented (Bistacchi and Massironi, 2000; Bistacchi et al., 2000).

The Col d'Olen Rock Glacier ("Corno Rosso 2 Rock Glacier" in the Aosta Valley rock glacier cadastre, http://www.geonavsct.partout.it) typology is talus-tongue shaped (Barsch, 1996) (rock glacier morphometric characteristics in Tab. 1). The surface of the rock glacier is covered by clasts (calcschists) varying from pluri-

decimetric to metric size (several boulders of tens of m^3 are also present), with large open voids between the fragments resulting in an edge-supported arrangement lacking interstitial fine debris. Fine-grained sediments (serpentinites) outcrop at the terminus and at the lateral scarps. The rock glacier seems to be active due to limited lichen growth, sparse vegetation, microform evidence of recent movement in the steep frontal slopes (e.g., small-size rockfalls and associated new deposit apron formations), in addition to load fresh and unstable boulders on the upper surface (Barsch, 1996; Millar and Westfall, 2008). The rock glacier is also classified as intact in the Aosta Valley rock glacier cadastre. The rock glacier shows a main flow direction from NE to SW, toward a small valley depression where the studied pond is located (Fig. 1d). The rock glacier does not have any surficial outflowing springs or streams.

The pond is situated in front of the rock glacier, on the right-marginal side of the tongue (Fig. 1d), showing an elongated shape in NE-SW direction (pond morphometric characteristics in Tab. 1). The pond shoreline is surrounded from NE to SE by the rock glacier, with the front dipping into the pond, from N to SW by weathering deposit slopes (scree accumulations and pedogenised fine-grained deposits often associated with alpine meadows) and a small rockfall deposit primarily composed of amphibolites, and it is partially bordered on the south by bare bedrock outcrop (calcschists). The pond has no stable surficial inflows. Only a tiny ephemeral snow melting stream is present, that usually disappears during the ice-free season (here defined as period with the pond ice-covered less than 50 % of its surface) in July-August. There are no surficial outflows. It is completely ice-covered during the winter season.

3. DATA AND METHODS

3.1 Ground Penetrating Radar (GPR)

Data acquisition

The GPR survey consisted of 17 profiles acquired using a 200-MHz IDS antenna, for a total length of 530 m, and 13 profiles employing a 500-MHz GSSI antenna, for a total length of 440 m (Fig. 2a). Both the surveys were carried out with an IDS K2 GPR unit. To acquire the profiles a flat-bottom plastic boat tracked with an Ublox EVK-686 GPS was used with an electric engine to maintain a constant speed. The same acquisition parameters were selected both for 200-MHz and 500-MHz antennas. The sampling frequency was 4 GHz with 2,048 samples per trace. Boat velocity and GPR scan rate, that was driven by the GPS at 3 readings/second, resulted in a trace interval equal to 0.02 m, on average.

Data processing

To understand the GPR pulse parameters (velocity, attenuation, wavelength) in pond water, water electromagnetic parameters were estimated. The dominant frequency of the pulse was estimated from spectra of reflections from the pond bottom. These signals were firstly isolated with a Hanning window (10 ns) centred at the maximum amplitude of reflection. Then, for both 200 and 500 MHz surveys, the average Fourier spectra were calculated for each profile. The maximum amplitude was found for both antennas corresponding to a frequency f = 200 MHz. The water electrical conductivity σ was about 50 μS cm^{-1}, based on several randomly located measurements in the pond, collected using a conductivity meter HI 98130 (HANNA instruments, accuracy at 20 °C of ±2 %, resolution of 10 μS cm^{-1}). At the bottom of the pond, pebbles and small blocks generate diffraction hyperbolas. To estimate the

velocity of the GPR pulse in water, 56 of these hyperbolas that were particularly clear and wide were selected. A mean value of about 34±0.5 x 10^{-3} m ns^{-1} was found, resulting in a relative permittivity ε_r of about 77.8±2.3 (considering the water lossless due to its very low conductivity). The uncertainty on velocity, together with that of the time picking (around 1 ns) give an uncertainty in water depth derivation of 0.05 and 0.20 m for the shallowest and the deepest reflections, respectively. Applying the Maxwell equations to the pond water, giving σ, f and ε_r, an intrinsic attenuation at 200 MHz equal to 0.93 dB m^{-1} and a dominant wavelength λ of about 0.17 m were calculated (Sambuelli and Bava, 2012). Only few diffraction hyperbolas with an average apparent velocity of about 45±1 x 10^{-3} m ns^{-1} were observed in the fine bottom sediments. Similar values have been found in the literature (e.g., Arcone et al., 2010). Assuming a relative permittivity of the solid mixture equal to 6.5 (Vaccaneo et al., 2004), and using the CRIM formula (Birchak et al., 1974), a porosity of approximately 65 % was obtained, that is likely attributable to a silty material. However, given the scarcity of diffraction events, the sediment thickness (Fig. 2c) was calculated using the velocity in water. In doing so, the sediment thickness was likely underestimated, and it could be from 1.2 to 1.4 times thicker than stated, depending on the true pulse velocity within the sediments.

The raw GPR data were processed with Reflexw software, using the following steps: i) spatial resampling of radagrams at equidistant traces of 0.02 m to keep a high-spatial resolution; ii) drift removal (zero time correction); iii) dewow to filter out low frequencies; iv) removal of average trace to attenuate ringing; v) spherical divergence compensation to recover the geometrical attenuation; vi) migration using the water velocity; and vii) muting above the pond bottom reflection. Within radargrams, fine sediment deposits showed organised parallel lines while pebbles

and rocks showed chaotic and waving reflections with broken and discontinuous phases due to scattering. The sediment-bottom reflections were picked only where the boundaries between ordered and chaotic reflections were clear. After assembling all the pickings, the bathymetry of the pond and the fine sediment thickness map were obtained (Fig. 2b and 2c). The depth values were gridded with triangular interpolation into a 10 cm x 10 cm mesh. From the high resolution DEM of the pond bottom, the hypsographic curve was obtained (Fig. 2d), and used for hydrological analyses.

3.2 Electrical Resistivity Tomography (ERT) and Self-Potential (SP)

Data acquisition

The electrical surveys were conducted with floating equi-spaced electrodes stretched across the pond in two different configurations (Fig. 3a): longer arrays were used along the main length of the pond (4 profiles with 48 electrodes 1.5-m spaced) while shorter arrays were used across the pond (4 profiles with 24 electrodes at 2-m spacing). Polyethylene foam floaters were used to allow the cables to be submerged. Cable takeouts were left directly in contact with water (Fig. 3b), obtaining fully submerged floating electrodes, while stainless steel electrodes were connected to the cable for measuring points on shore. Each of these last electrodes was geo-referenced using an Ublox EVK-686 GPS to record the position of the survey line. For both configurations, a Wenner-Schulumberger sequence was adopted, with a total of 545 measuring quadrupoles for long arrays and 126 for short arrays, to take advantage of both vertical and lateral resolution. A multichannel resistivity meter (Syscal Pro - Iris Instruments) was used for data acquisition.

The Syscal-Pro also allowed for a contemporary acquisition of SP data which were later mapped along the pond. In particular, the SP data were collected along the ERT lines 1, 2, 3 and 4 (electrode spacing 1.5 m), which were the longest available survey lines along the lake (Fig. 3a). SP potentials were measured for each multiple of the electrode spacing obtaining SP values with different separation of potential measuring electrodes (1.5, 3, 4.5, 6 m).

Data processing

ERT data were inverted with the software Res2DInv (Geotomo Software). To focus the inversions in both the sediments below the water and in the underlying bedrock a strong a-priori constraint was imposed to depth and resistivity of the water layer. A constant resistivity was then imposed to the shallower elements of the model until an appropriate water depth to reflect the water layer presence. Only the lower part of the model was therefore used for the evaluation of the sub-bottom resistivity distribution. In this way, the inversion program only iterates on the resistivity of the lower part of the model, with a fixed water layer above, to obtain more realistic resistivity values for sediments and rocks. For robust inversion in water covered environments, the water column resistivity and its geometry must indeed be known accurately as a large portion of the electric current may flow through the water layer (Loke and Lane, 2004). This can be considered using a distorted finite-element grid to calculate apparent resistivity (to be compared with the acquired data) with the nodes along the bottom row of the water mesh adjusted to match bathymetry. Water resistivity was imposed based on the mean apparent resistivity measured with electrodes having the shortest spacing. These raw data showed a consistent and spatially homogeneous electrical resistivity as confirmed also by several independent

randomly located measurements carried out with the conductivity meter HI 98130. The water resistivity was about 200 Ohm·m, with this relatively high value a good penetration of current lines in the bottom sediments is allowed.

The SP data obtained with the potential electrode separation of 3 m have been used for mapping. This separation has been chosen to reduce short wavelength noise in raw data and to focus on potential anomalies near the bottom of the lake, having an electrode separation similar to the maximum water depth. A total of 130 SP values were mapped after a gridding with triangulation on a 2 m x 2 m mesh, and filtered with a Gaussian 3 x 3 square filter to smooth the map and enhance larger scale anomalies.

3.3 Lacustrine sediment properties

Lacustrine sediment probing

Lacustrine sediments were analysed to support the results obtained from the geophysical investigations. Grain size, sulphur concentrations and electrical conductivity were analysed to compare the laboratory data with the potential porosity value obtained by GPR data processing and resistivity values derived from ERT. To do this, two 10-cm-long surficial fine sediment cores were collected from the pond bottom using a boat anchored to the pond shores to ensure enough stability during the coring activities, and a Beeker vibracore sampler (Eijkelkamp, NL), equipped with a polyethylene tube with a diameter of 6 cm and a 2-m steel extension at the top of the sampler to reach the bottom of the pond. The core locations (Fig. 2c) were selected using the GPR-derived sediment thickness map to identify sites undisturbed by boulders and pebbles.

Laboratory analyses

Samples were immediately sealed with a tight stopper to avoid oxygen infiltration and stored at 4 °C until laboratory analysis. The presence of sulphidic material was observed through the colour response of the matrix after adding some drops of 3 % H_2O_2 and by recording the odour description of each sample (Fanning and Fanning, 1989; Fanning et al., 2002; McVey et al., 2012). The samples were then air-dried and sieved to 2 mm (Balduff, 2007), and sediment particle size distribution was determined by pipette method (Gee and Bauder, 1986). A wet subsample of each core was aerobically incubated for 16 weeks in 1:1 (w:v) soil:distilled water in order to detect the lowering of pH due to acid sulphate weathering oxidation in soil horizon which contain reduced sulphides (Bradley and Stolt, 2003; McVey et al., 2012). Total S (TS) was quantified by ICP-OES (Ametek, Germany) after aqua regia digestion in a Millestone 1200 microwave oven (Vittori Antisari et al., 2011). Finally, electrical conductivity measurements were performed using a VWR Multi 340i - WTW multimeter (accuracy ±0.5 %, resolution 1 µS cm^{-1}).

3.4 Hydrological regime

Air temperature, snow height, atmospheric pressure, relative humidity and wind speed were measured at the Col d'Olen AWS (automatic weather station, 2900 m a.s.l.) located at about 800 m distance from the pond. Rain data were obtained from the Gressoney-La-Trinité - Lago Gabiet AWS (2379 m a.s.l.), which is located 2.5 km from the pond. Direct short wave radiation data were extracted from the Bocchetta delle Pisse meteorological station (2410 m a.s.l.) located ca. 3 km far from the pond. Hourly meteorological data were aggregated to daily values and used for the

hydrological analyses in the investigated ice-free periods 2014 (July-October) and 2015 (June-October).

Water level was measured approximately on weekly basis during the ice-free seasons using a hydrometric station with direct observations. The pond watershed area (206,000 m^2) was delineated using a Digital Terrain Model (DTM, cell size: 2 m x 2 m) produced by Regione Autonoma Valle d'Aosta. The surface area of the rock glacier contributing to the pond watershed is 21,800 m^2 i.e., 10.6% of the whole watershed.

During the two observed years, a clear dominance of liquid precipitation during the ice-free seasons was observed. This allowed avoiding the application of a snow-melt model in calculating pond inflow during the ice-free periods. This was obtained as the difference between the precipitation and the evapotranspiration calculated applying the Penman-Monteith method (Penman, 1948; Monteith, 1985) on the whole basin. The pond volume fluctuations were computed from bathymetry and monitored water level. The ice-free season pond outflow could not be monitored directly due to the lack of a surface flow. Instead, it was calculated as the difference between ice-free season mean inflows and pond volume fluctuations.

3.5 Water temperature measurements, heat tracers and electrical conductivity measurements

To explore the thermal stratification, temperature profiles were measured using an inflatable boat and a hand-held portable thermometer HI 98130 (HANNA instruments, accuracy ±0.5 °C, resolution 0.1 °C). Measurements were performed twice, on 12 July and 6 September 2015, investigating from the epilimnion to the deepest part at 20, 100, 200 and 300 cm depth.

Water temperature in the pond was continuously measured during the water sampling periods at three sites in the pond (Fig. 2b) defined as RG1-RG2-RG3 (25 August - 9 October 2014; 9 July - 12 October 2015). Miniature temperature loggers Onset HOBO® TidbiT v2 Temp loggers (accuracy ±0.21 °C, resolution 0.02 °C) (RG1) and Maxim iButton® DS1922L (accuracy ±0.5 °C, resolution 0.0625 °C) (RG2 and RG3) were programmed to record every three hours. Loggers were installed at the pond bottom about 3-5 m from the shoreline at 1.5 m (RG1 and RG3) and 1.8 m (RG2) depth, placed at the sediment-water interface, among blocks (diameter 25-60 cm) to shield them from direct solar radiation. RG3 was placed in an area into the pond showing maximum SP values (potential sub-surface inflow); RG2 was installed in an area with minimum SP values (potential sub-surface outflow); RG1 was placed far from the rock glacier in order to detect and quantify the thermal influence of a potential inflow coming from the rock glacier and affecting the closest sensors (RG2 and RG3), in an area with SP values close to 0 mV (likely absence of flow).

The total daily discharge flow into the pond (Q_{tot_i}) can be calculated as the sum of the rock glacier discharge (Q_{rock_i}) and all other possible inputs (effective precipitation, run off, sub-surface flow, etc.) (Q_{ext_i})

$$Q_{tot_i} = Q_{ext_i} + Q_{rock_i} \quad (1)$$

In this equation, the three terms are unknown. The absence of surface inflows and outflows does not allow to derive the rock glacier discharge. In this context, a classical water balance approach at daily scale would not help in determining these parameters. Conversely, calculation of the pond energy balance using heat tracer

allows to obtain more information on the contributions of rock glacier inflow to the pond.

The energy balance of the pond can be written as

$$c_w \varphi_w T_{3_i} Q_{tot_i} = c_w \varphi_w T_{2_i} Q_{ext_i} + c_w \varphi_w T_0 Q_{rock_i} \quad (2)$$

where φ_w (kg m^{-3}) is the density of water, c_w (J kg^{-1} K^{-1}) is the specific heat of water, T_{2_i} and T_{3_i} are RG2 and RG3 temperatures (°C) at the i_{th} day, and T_0 is the meltwater temperature of the rock glacier. RG3 and RG2 were chosen because of their locations, one in correspondence of strong positive SP values (RG3) and one located in an area with strong negative SP values (RG2). The eq. 2 has been used for estimating the relative rock glacier discharge with meltwater temperature at -0.5 °C, +0 °C and +0.5 °C, and assumed constant over time (e.g., Krainer et al., 2007; Millar et al., 2013). A negative water temperature was chosen as lower threshold considering the accuracy of the sensors deployed in the pond and due to possible freezing point depression from dissolved salts (e.g., Banin and Anderson, 1974; Davis, 2001). Both c_w and φ_w are constant and thus can be neglected (Langston et al., 2013).

To solve the problem of the unknown terms Q_{tot_i} and Q_{ext_i}, Q_{tot_i} was posed = 1 for all considered days, deriving the eq. 3 as function of Q_{rock_i}

$$T_{3_i} = T_{2_i}(1 - Q_{rock_i}) + T_{0_i} Q_{rock_i} \quad if\ Q_{tot_i} = 1 \quad (3)$$

Then, Q_{rock_i} has been obtained as function of T_{3_i} and T_{2_i}. However this simplification induces a loss of information. In fact, Q_{rock_i} in the resulting eq. 4 is not expressed as daily absolute value of the discharge coming from the rock glacier, but it represents the rate of rock glacier discharge on total discharge reaching the RG3 sensor in i_{th} day.

$$Q_{rock_i} = \frac{T_{3i} - T_{2i}}{T_{0i} - T_{2i}} \quad if\ (T_{3_i} \leq T_{2_i}\ and\ T_{3_i} \geq \mathrm{T}_0)\ => 0 \leq Q_{rock_i} \leq 1 \quad (4)$$

The application of this approach allows to know the periods when the contribute of rock glacier is conspicuous. However, in absence of further hydrological balance terms such as inflow runoff or pond outflow, that is a common deficiency at all high-elevated water bodies, this method provides evaluable qualitative information (eq. 4), although it is not able to quantify the rock glacier contribution in absolute terms.

Finally, to characterised the chemical signature of the pond on spatial and temporal basis, water samples were collected on weekly basis in correspondence of the water temperature measurement sites (RG1-RG2-RG3). Samples were collected in 50-ml Falcon tubes, stored in an ice-packed cooler (KERN FRIO Diagnosach) during car transport and immediately transferred to the laboratory where they were analysed for electrical conductivity (EC) (Crison - Micro CM 2201), used as proxy of solute load.

4. RESULTS

4.1 Geophysical evidence

GPR

The GPR tracks clearly show a series of dense diffractions along the pond eastern bank, parallel to the rock glacier front, characterised by a rough surficial appearance (Fig. 4a). The coarse diffractions progressively disappear towards the centre of the pond, ending in a bouldery apophysis located at ca. 5-7 m distance from the shore (Fig. 4b). In the southeastern corner of the pond, the waterborne GPR profiles highlight the presence of surficial coarse diffractions mixed to a generally smooth-reflecting horizon at shallow depths, indicating the potential presence of a boulder-rich fine-grained deposit composed by blocks from the rock glacier and fine-grained lacustrine sediments (Fig. 4b).

From the bathymetric and fine-sediment thickness maps (Fig. 2b and 2c), a directional depression pattern can be observed in the central and northern parts of the pond, showing a N-S preferential elongated orientation, where water depth and fine-sediment thickness are greater. This elongated depression can be seen in the GPR track shown in Fig. 4c and 4d, which highlights an evident asymmetrical structure of this pond section. Slopes are greater along the rock glacier front in the East whereas the western portion of the pond is characterised by a shelf area, where the bottom surface is nearly horizontal and generally beneath less than 1.2 m of water.

ERT and SP

In Fig. 5 the results of the 2D inversion along some selected lines are reported (for line locations see Fig. 3). For all the sections, given the good electric coupling of

injecting and measuring electrodes, high quality data were acquired. The resulting RMS % difference between measured and calculated apparent resistivities in the inverse problem was always below 2.3 %. On each imaged section, bathymetry and sediment thickness are shown (Fig. 2b and 2c). Most of the ERT lines resolve an underwater layer of sediments with a thickness well matching GPR data. Remarkably, this thickness information was not included as a constraint in the inversion, therefore, the coherence of the two results is an indication of the goodness of the performed inversion. The sediments just below the bottom of the pond have a resistivity (about 150 Ohm·m) lower than one of the water layer (200 Ohm·m). Laboratory measurements of electrical conductivity of the two surface lacustrine sediment samples are coherent with the results obtained from the resistivity surveys.

Beneath the low-resistivity lacustrine sediment layer, the pond bed does not show horizontally constant resistivity values. From the ERT results it is evident that higher resistivity values in the sub-sediment zones are in the northern part of the pond (1000-4000 Ohm·m), while in the southern zones a strong continuous anomaly (3000-5000 Ohm·m) is located at the pond margin and on the shore (Fig. 5). Moreover, most survey lines report a wide zone with relatively low resistivity (300-600 Ohm·m) truncating the two higher resistive areas. For the line nearest to the rock glacier (L1, close to the southern shore), this anomaly is concealed (Fig. 5) probably due to 3D effects. A 3D fence diagram of the ERT results is also reported in Fig. 6; from this representation, it is possible to understand the good correspondence of the inverted resistivity values at the lines intersections and the orientation of the low resistivity anomaly within the bedrock. From this last representation, a plan view of the 2000 Ohm·m isosurface, obtained by 3D interpolation of the resistivity data is compared with the SP map (Fig. 7). The SP map shows a remarkable spatial

coherency of maxima and minima in NW-SE bands that correspond with the ERT results. A good agreement with the minima of SP and the NW-SE band with low resistivity values is evident if the volumes with resistivity higher than 2000 Ohm·m are plotted (Fig. 7b). In Fig. 7b the low resistivity discontinuity is clearly visible as a WNW-ESE elongated band affecting the pond bedrock for a width between 10 and 15 m. SP results evidence the presence of 4 low potential anomalies indicated by negative potentials (-10 to -120 mV), with a similar orientation of the low resistivity discontinuity. The SP map has been obtained from L1-L4 SP profiles, showing a good alignment of maxima and minima. Thus, giving the unlikely occurrence of a replica of the same artefact in all the acquired profiles, we consider this spatial SP pattern to be related to the geological structure beneath the pond. One main negative band (minimum: -120 mV) was detected along the resistivity anomaly identified by the ERT investigations. One main positive anomaly (maximum: 300 mV) was found in the northern part of the pond (Fig. 7a). A secondary slightly positive anomaly was found on the southern shore of the pond. In this area, the SP data were obtained measuring between one electrode in the ground and the other floating in water. A different salinity in underground water and pond water could contribute to the build-up of this potential. Thus, it is considered as an artefact in this context of analysis.

Lacustrine sediment properties

The granulometric analyses show that the sample n°1 (CL1 in Fig. 2c) is mainly composed of silt (82.8 %), sand (9.6 %) and clay (7.6 %). Sample n°2 (CL2 in Fig. 2c) is similar with silt (82.9 %), sand (11.8 %) and clay (5.3 %). Since sediments are mainly composed of silt, the 65 % porosity for the GPR data is reasonable (e.g., Das,

2008). The sediments appear dark brown to black coloured with a strong sulphidic odour, suggesting the presence of organic sulphur compounds. The evidence of sulphidation process was further demonstrated by acidification during aerobic incubation (Ferronato et al., 2016), which occurred in both the samples, losing up to 1.8 pH units. The accumulation of reduced organic S compounds was also confirmed by high TS content measured in the two cores (0.6 g kg^{-1} - CL1 and 0.4 g kg^{-1} - CL2). Furthermore, laboratory measurements of electrical conductivity of the two samples reported a mean value of 62 µS cm^{-1} (i.e., 161 Ohm·m). This value is in accordance with the ERT results for the same layer (around 150 Ohm·m). The high silt content and the presence of organic material could explain why the overall resistivity within the samples is lower than the water (200 Ohm·m) in the resistivity sections. This result is similar to some published data (Mitchell et al., 2008; Nyquist et al., 2008; Colombero et al., 2014).

4.2 Hydrology

Hydrological regime

The liquid precipitation during the ice-free seasons 2014 and 2015 was 478 mm and 567 mm (Fig. 8a and 8b). A continuous water level decrease was observed during the weekly hydrological observations, reaching the minimum at the end of the ice-free season, with almost the same drop of 30 cm in both 2014 and 2015 (Fig. 8c and 8d). During the investigated periods, independent from the precipitation amount, the pond showed a continuous decrease in water level, suggesting the presence of continuous seepage. In fact, water lost during the ice-free periods 2014 and 2015 is -0.05 L s^{-1}, on average (estimated considering a mean decrease of 30 cm in water lever). The ice-free season mean inflow was calculated equal to 7.17 L s^{-1}.

Therefore, the outflow is likely (7.22 L s^{-1}) similar to the inflow, indicating that the loss of volume is insignificant compared to the incoming and outgoing flows. This, in turn, points to sub-surface seepage as a likely outflow mechanism.

Water temperature measurements, heat tracers and conductivity measurements

The water temperature profiles in the deepest zone of the pond were approximately isothermal both on 12 July and 6 September 2015, showing a slight temperature decrease toward the bottom (300 cm depth) of 0.9 °C and 0.8 °C (Tab. 2). Thus, the pond is not thermally stratified during the ice-free season.

Fig. 9a and 9b show daily air and water temperature trends for RG1, RG2, and RG3 during the two ice-free seasons (2014-2015) and Fig. 9c and 9d report precipitation. The difference between RG1 and RG2 is low (0.18 °C, on average). Conversely, in the same periods the difference between RG3 and RG1-RG2 can reach 10 °C.

The difference between RG2 and RG3 can be used to infer the water coming from the rock glacier. Assuming that its temperature is constant, the temperature at RG3 is the result of a heat balance between heat flow coming from the rock glacier and heat stored in the lake (RG2). The cold water flux from the rock glacier, expressed as ratio between the discharge of the rock glacier and the total runoff reaching the pond, was investigated through heat tracers. Results show that in 2014 the main contribution of the rock glacier can be observed from mid-September until mid-October (Fig. 9e), in 2015 it is one month earlier (mid-August until mid-September) (Fig. 9f). In both cases the maximum contribution is observed before the air temperature becomes negative or close to 0 °C. It was also observed that highest

contributions from the rock glacier detected in the pond were often associated with precipitation events.

Increased electrical conductivity was found to correlate with increasing contributions from the rock glacier at RG3. During these periods, electrical conductivity values were up to almost twice at RG3 site than at RG1 and RG2 sites (Fig. 9g and 9h).

5. DISCUSSION

5.1. Structural setting

The GPR tracks show rough diffractions along the eastern bank, parallel to the rock glacier front, which were interpreted as the bouldery rock glacier tongue flowing into the pond (Fig. 4a). These coarse diffractions progressively disappear towards the centre of the pond ending in a bouldery apophysis (Fig. 4b). This represents the deep foot of the rock glacier that flows into the pond perimeter. This evidence together with the asymmetrical structure of the pond (Fig. 4c and 4d) suggest that the advancing movement (creep) of the rock glacier has progressively filled the small valley depression in which the pond is located, emphasizing its “V” shape.

No evidence of deformed features was found in the fine lacustrine sediments along the rock glacier front (Fig. 4c and 4d), suggesting that the landform has progressively moved down on the slope and buried the lacustrine sediments (and the material coming from the rock glacier front) on the eastern side of the pond instead of pushing them during its advance. This is in agreement with the description of rock glacier movement where material is transported towards and down the rock glacier fronts, then incorporated at the bottom of the advancing permafrost body, and finally, overridden by it (Kääb and Reichmuth, 2005).

The advancing of the rock glacier has also generated a small deposit apron in a flat zone of the southeastern area of the pond (Fig. 10). Here the waterborne GPR profiles highlight the presence of surficial coarse diffractions mixed to a generally smooth-reflecting horizon at shallow depths, indicating the potential presence of a boulder-rich fine-grained deposit composed by boulders from the rock glacier and fine-grained lacustrine sediments (Fig. 4b). ERT surveys show that in this area a body of massive bedrock is present (3000-5000 Ohm•m), partially outcropping towards the southwestern side (Fig. 10). Thus, it is assumed that the southern shore is composed by bare bedrock in the western portion, and partially by sub-surface bedrock with overlaying rock glacier deposits in the southeastern corner. Here, the rock glacier apron at the surface lies on the sub-surface bedrock. Thus, it is possible to assume that the advancing of the rock glacier might have influenced the evolution of the pond, creating a small dam which might have contributed in increasing the level of water impounded in the valley depression (Fig. 11a1 and 11a2).

Lacustrine sediments in the northern part of the pond show a rather continuous pattern over the high-resistivity body (Fig. 5, L1-L4); conversely, in the central and southern part of the pond sediments show some discontinuities (Fig. 5, L1-L4). This structural setting corresponds to a sharp change in the bedrock properties below pond sediments. Sharp vertical contacts between bedrock units are aligned with discontinuities in the lacustrine sediments. Based on observations of litho-structural properties of bedrock units in several outcrops around the Col d'Olen and rock glacier area (Fig. 12a and 12b), these vertical structures could correspond to a highly-fractured rock mass developed across a shear zone due to a major N100E fault. Evidence of tectonic deformations can also useful for understanding

hydrogeological properties of bedrock which could constrain inflow and outflow dynamics, as discussed in the following sections.

5.2. Seepage

The ERT data show a wide zone with relatively low resistivity (300-600 Ohm·m) truncating two higher resistive areas. This low-resistivity area shows a WNW-ESE elongated orientation in the pond bedrock for a width of about 10-15 m (Fig. 5, 6 and 7b). The orientation of the low resistivity is in accordance with the orientation of distinctive structural association of brittle faults and fractures in the area. Indeed, Bistacchi and Massironi (2000) and Bistacchi et al. (2000) reported that the geological context of the study area is highly affected by WNW-ESE Miocene-to-Present fault lineaments. The sharp morphology of the low-resistivity anomaly, the strong resistivity contrast, and the orientation of this structure considering the general structural setting of the area, suggest that this could be related to a minor fault zone affecting the bedrock. Within this fault zone resistivities values are lower than the surrounding bedrock due to the higher water content of altered and highly fractured rocks. This area of weakness could therefore significantly affect the water balance through modification of the water circulation from the pond by seepage.

Remarkably, the main negative SP area was found along the anomaly detected by the ERT analyses (Fig. 7a), thus a water seepage from the pond can be assumed to occur at this location (Fig. 11b and 11c). This finding supports the hypothesis of a continuous seepage throughout the ice-free seasons 2014 and 2015, independent from precipitation. The regional character of the fault zone (Bistacchi and Massironi, 2000; Bistacchi et al., 2000) indicates a possible deep extension of its shear zone. Deep-seated fractured bedrock below the pond could deeply absorb outflowing water

from the pond, thus preventing local superficial evidence of outflow patterns, which in fact were not observed downstream the pond.

Due to the isothermal conditions of the pond both in July and September 2015, the presence of a conspicuous inflow of cold water coming from the rock glacier and flowing at the pond bottom can be excluded. Indeed, this should result in a strong thermal stratification with cold waters flowing towards the fractured zone at the pond bottom, which is inconsistent with the observation of a completely mixed pond. Thus, water inflow coming from the rock glacier is assumed to be reduced, as also discussed in the following section.

5.3. Inflow

The pond water level decreased rather continuously throughout the ice-free seasons 2014 (Fig. 8c) and 2015 (Fig. 8d), with limited periods of level increase due to strong precipitation. Even during warm atmospheric periods, such as mid-August - mid-September 2014 and mid-July - early August 2015, water level in the pond showed decreasing trends. This evidence preliminarily suggests that the melting of internal ice in the rock glacier did not contribute consistently in the hydrological regime of the pond during the investigated ice-free seasons. Indeed, an increase in air temperature should result in increasing amount of meltwater exported into the pond due to enhanced ice melting, leading to increases in water level (Langston et al., 2013). Conversely, the observed pattern is in agreement with the results obtained by previous studies on rock glacier hydrology (Berger et al., 2004; Krainer and Mostler, 2002; Krainer et al., 2007; Geiger et al., 2014). These researches reported gradual decline in rock glacier discharge throughout the summer (with the

progressive depletion of the snowpack) except during storms, with a minimum contribution of icemelt to the total discharge on seasonal basis.

The SP results show one main positive anomaly located in the northern part of the pond, close to the rock glacier (Fig. 7a). The RG3 sensor was placed at this site and recorded much lower water temperatures than in other parts of the pond (RG1 and RG2). Cold water coming from active rock glaciers has been recorded in previous studies and attributed to the effect of direct contact of water to an ice or permafrost body, and/or ground ice melting (e.g., Haeberli, 1975; Krainer and Mostler, 2002; Berger et al., 2004; Williams et al., 2006; Krainer et al., 2007; Krainer et al., 2012; Millar et al., 2013; Carturan et al., 2016). Moreover, the litho-structural setting of the slopes in the rock glacier area and sedimentology of the pond suggest that high density and persistence of structural discontinuities (N100E and N60E systems) make permeable the rock masses in the northern side of the pond, thus limiting runoff and preventing surficial flow. The impermeable character of sub-surface high resistivity bedrock (Fig. 7b, zone C) and the absence of vertical discontinuities in pond sediments (Fig. 5, L1-L4) in its northern side should also impede pond to be fed by underground water, which could be absorbed by fractured bedrock along the shear zones. For these reasons, the main SP positive anomaly was exclusively attributed to the evidence of cold water flowing from the rock glacier into the pond (Fig. 11b and 11c).

Since only RG3 is characterised by cold water, it is possible to assume that the pond is well mixed, as also demonstrated by water temperature profiles (Tab. 2), and that the cold source located in proximity of RG3 lowers temperature only in its proximity (Fig. 9a and 9b). Even if the temperature of the cold source is low (<= +0.5 °C), its discharge can be reduced. Therefore, the influence of the cold source on

RG2 (and RG1) temperatures is negligible. This agrees with previous observations of rock glacier outflows, which are characterised by small discharge because debris layers protect rock glaciers ice from solar radiation and strongly reduce ablation rates (Potter, 1972; Gardner and Bajewsky, 1987; Krainer and Mostler, 2002; Millar et al., 2013).

Heat tracer results show that in 2014, the main contribution of the rock glacier is from mid-September to mid-October (Fig. 9e), in 2015 it is one month earlier (mid-August to mid-September) (Fig. 9f). Warmer air in July-August 2015 (mean: +6.4 °C) in comparison to July-August 2014 (mean: +3.4 °C) could have influenced the thawing of the rock glacier. Moreover, warmer air in September 2014 (mean: +2.5 °C) than September 2015 (mean: -0.1 °C) probably contributed to extending the thawing season until October 2014. The contribution from the rock glacier reaches minimum values when mean air temperature is negative or close to 0 °C for some days, as is especially evident in 2015. This marks the end of the rock glacier cold water export at the end of the ice-fee season and the cold water source could be frozen or characterised by an extremely small discharge (Krainer and Mostler, 2002; Krainer et al., 2012; Millar et al., 2013).

Main contributions from the rock glacier were found to often be associated with precipitation during the ice-free season, which increased the export of cold water from the landform (Krainer and Mostler, 2002; Berger et al., 2004). This resulted in a clear decrease of water temperature at RG3 (Fig. 9a and 9b) due to the greater amount of cold water flowing into to the pond (Fig. 11d).

A correlation between rock glacier contribution peaks and increases of electrical conductivity monitored at RG3 on weekly basis was observed (Fig. 9g and 9h). These results agree with previous studies, which attributed increases in electrical

conductivity to the export of highly-mineralised waters from ice melting and groundwater in rock glaciers, especially at the end of the ice-free season (e.g., Williams et al., 2006). At the beginning of the ice-free season 2015 (from mid-July to mid-August), water temperatures at RG3 were colder (ca. 7 °C on the average) than at RG1 and RG2 sites. However, electrical conductivity was not found to be higher at RG3, as happened during previously described periods of higher rock glacier contributes. This evidence was attributed to the potential presence of long-lasting snow patches melting among the boulders of the rock glacier, which contributed in exporting cold and chemically-low concentrated water fluxes into the pond (Williams et al., 2006).

Since electrical conductivity peaks chiefly occurred with cold water inflows driven by precipitation, it is possible to assume that the infiltration of rain water in the ice-sediment matrix might be able to increase rock glacier-ice melting, enhancing the export of mineralised waters (Fig. 11d). This process must be considered when studying the role of rock glaciers in influencing surface water hydrology and physiochemistry in high-mountain watersheds. Thus, further in-depth physiochemical analyses aimed to understand the processes driving the export of enriched-solute fluxes from rock glaciers are required, considering the small number of studies that investigated the potential negative effects of rock glacier thawing on surface water in mountain regions (Thies et al., 2007; Ilyashuk et al., 2014).

CONCLUSIONS

The present work provides new insights into the mechanisms linking active rock glaciers and impounded surface waters in high-mountain areas through the integration of waterborne geophysical techniques and heat tracers.

On the basis of the performed surveys we hypothesise that the advancing movement of the rock glacier has modified the configuration of the valley depression, where the pond is located, which has been progressively filled by the rock glacier. Rock glacier advance is also assumed to have modified the level of water impounded in the depression, through the creation of a dam. The hydrological connection between the rock glacier and the pond is represented by a sub-surface hydrological window where an inflow of cold and mineralised underground waters released from the rock glacier was observed. Greater water contribution from the rock glacier occurred following intense precipitation events during the ice-free season, with concomitant increasing electrical conductivity values. The outflow of the pond is dominated by a sub-surface seepage within a minor fault zone, characterised by the presence of altered and highly-fractured rocks in the bedrock, related to the geological history of the area.

The proposed investigation approach has been demonstrated to be useful for a better understanding of the dynamics governing geological and geomorphological settings similar to the one studied. Regarding the geophysical methods, successful experience has been obtained for the characterisation of wider lakes and for the reconstruction of underwater geological environments (Sambuelli et al., 2011; Sambuelli and Bava, 2012; Colombero et al., 2014). When lake dimensions increase, waterborne ERT can be easily conducted pulling the electric cable by boat and acquiring several measurements to be inverted in an unique dataset. Acquisition and processing of GPR data follow similar procedures to ones presented in this paper. From the acquisition point of view, timing and costs are not an issue since several kilometres of both GPR and ERT data can be acquired simultaneously within a single working day. To validate the hydrological observations obtained by

geophysical measurements, the application of heat tracers is recommended. Clearly, the increase of the investigation areas and water depths requires a subsequent increase of monitoring points and usually more complicated analyses have to be undertaken to fully understand the flow dynamics, especially when the quantification of groundwater discharge is desired (Schmidt et al., 2007; Constantz, 2008; Langston et al., 2013). Although further testing of the proposed approach is required, it is evaluated here as a suitable technique for investigating logistically-complex hydrological settings which could be possibly transferred to wider scales of investigation.

ACKNOWLEDGMENTS

We would like to thank Maria Martin, Emanuele Pintaldi, Diego Franco, Danilo Godone, Elisa Giaccone and Elena Serra for their help in data acquisition, field work activities and laboratory analyses. We are also grateful for the support given by Simona Fratianni (Department of Earth Sciences, University of Turin, Italy), Michele Freppaz, Michele D'Amico and Roberta Gorra (Department of Agricultural, Forest and Food Sciences, University of Turin, Italy), Lino Judica and Adriana Bovio (Territorial Laboratory of Environmental Education, University of Turin, Italy), Ernesto Colombo, Lorena Bulla and Carina Schuh. Finally, we give special thanks to the family Beck-Peccoz, Consorzio di Miglioramento Fondiario di Gressoney (Aosta) and MonteRosa-ski. This research has been partially funded by PRIN 2010-11 (project of the Italian Ministry for Education and Research) named "Dinamica dei sistemi morfoclimatici in risposta ai cambiamenti globali e rischi geomorfologici indotti" (coord. Prof. Carlo Baroni). AE and two anonymous reviewers provided valuable feedback and input during the discussion stage of this manuscript.

REFERENCES

Anderson MP. 2005. Heat as a ground water tracer. Ground Water 43(6) : 951-968.

Arcone S, Finnegan D, Boitnott G. 2010. GPR characterization of a lacustrine UXO site. Geophysics 75(4) : 221-239.

Azócar GF, Brenning A. 2010. Hydrological and geomorphological significance of rock glaciers in the dry Andes, Chile (27°-33° S). Permafrost and Periglacial Processes 21 : 42-53.

Balduff DM. 2007. Pedogenesis, inventory, and utilization of subaqueous soils in Chincoteague Bay. University of Maryland: Maryland.

Banin A, Anderson DM. 1974. Effects of salt concentration changes during freezing on the unfrozen water content of porous materials. Water Resources research 10(1) : 124-128.

Barsch D. 1996. Rockglaciers: Indicators for the Present and Former Geoecology in High Mountain Environments. Springer-Verlag: Berlin-Heidelberg.

Befus KM, Cardenas MB, Ong JB, Zlotnik VA. 2012. Classification and delineation of groundwater-lake interactions in the Nebraska Sand Hills (USA) using electrical resistivity patterns. Hydrogeology Journal 20 : 1483-1495.

Berger J, Krainer K, Mostler W. 2004. Dynamics of an active rockglacier (Ötztal Alps, Austria). Quaternary Research 62 : 233-242.

Birchak JR, Gardner CG, Hipp JE, Victor JM. 1974. High dielectric microwave probes for sensing soil moisture. Proceedings of the IEEE 62 : 93-98.

Bistacchi A, Massironi M. 2000. Post-nappe brittle tectonics and kinematic evolution of the north-western Alps: an integrated approach. Tectonophysics 327 : 267-292.

Bistacchi A, Eva E, Massironi M, Solarino S. 2000. Miocene to present kinematics of the NW-Alps: evidences from remote sensing, structural analysis, seismotectonics and thermochronology. Journal of Geodynamics 30 : 205-228.

Bradley MP, Stolt MH. 2003. Subaqueous soil-landscape relationships in a Rhode Island Estuary. Soil Science Society of America Journal 67 : 1487-1495.

Brenning A. 2005. Geomorphological, hydrological and climatic significance of rock glaciers in the Andes of Central Chile (33-35°S). Permafrost and Periglacial Processes 16 : 231-240.

Burger KC, Degenhardt JJ, Giardino JR. 1999. Engineering geomorphology of rock glaciers. Geomorphology 31 : 93-132.

Carturan L, Zuecco G, Seppi R, Zanoner T, Borga M, Carton A, Dalla Fontana G. 2016 Catchment-scale permafrost mapping using spring water characteristics. Permafrost and Periglacial Processes 27(3) : 253-270.

Colombero C, Comina C, Gianotti F, Sambuelli L. 2014. Waterborne and on-land electrical surveys to suggest the geological evolution of a glacial lake in NW Italy. Journal of Applied Geophysics 105 : 191-202.

Corte A. 1976. The hydrological significance of rock glaciers. Journal of Glaciology 17 : 157-158.

Constantz J. 2008. Heat as a tracer to determine streambed water exchanges, Water Resources Research 44(4). DOI:10.1029/2008WR006996/full.

Dal Piaz GV. 2001. Geology of the Monte Rosa Massif: historical review and personal comments. Schweizerische Mineralogische und Petrographische Mitteilungen 81 : 275-303.

Das B. 2008. Advanced Soil Mechanics. Third Edition, Taylor & Francis: London & New York.

Davis N. 2001. Permafrost: a guide to frozen ground in transition. University of Alaska Press, Fairbanks.

Fanning DS, Fanning MCB. 1989. Soil: Morphology, Genesis, and Classification. John Wiley & Sons: New York.

Fanning DS, Rabenhorst MC, Burch SN, Islam KR, Tangren SA. 2002. Soil Mineralogy with Environmental Applications. SSSA: Madison, WI.

Ferronato C, Falsone G, Natale M, Zannoni D, Buscaroli A, Vianello G, Vittori Antisari L. 2016. Chemical and pedological features of subaqueous and hydromorphic soils along a hydrosequence within a coastal system (San Vitale Park, Northern Italy). Geoderma 265 : 141-151.

Gardner, J.S., Bajewsky, I. 1987. Hilda rock glacier stream discharge and sediment load characteristics, Sunwapta Pass area, Canadian Rocky Mountains. [Eds.] Giardino, J.R., Shroder, J.F., Vitek, J.D., Rock Glaciers. Allen and Unwin, London, 161-174.

Gasco I, Borghi A, Gattiglio M. 2011. P-T Alpine metamorphic evolution of the Monte Rosa nappe along the Piedmont Zone boundary (Gressoney Valley, NW Italy). Lithos 127(1-2) : 336-353.

Gee GW, Bauder JW. 1986. Methods of soil analysis: part 1 - physical and mineralogical methods, SSSA book series. Soil Science Society of America, American Society of Agronomy.

Geiger ST, Daniels JM, Miller SN, Nicholas JW (2014). Influence of rock glaciers on stream hydrology in the La Sal Mountains, Utah. Arctic, Antarctic, and Alpine Research 46(3) : 645-658.

Goto T, Kondo KK, Ito R, Esaki K, Oouchi Y, Abe Y, Tsujimura M. 2012. Implications of self-potential distribution for groundwater flow system in a nonvolcanic mountain slope. International Journal of Geophysics. DOI: 10.1155/2012/640250

Grangeia C, Matias M. 2012. Shallow water integrated geophysical survey - a case study with geological and hydrological consequences. Proceeding of Near Surface Geoscience - 18th European Meeting of Environmental and Engineering Geophysics, DOI: 10.3997/2214-4609.20143407.

Gubler S, Fiddes J, Keller M, Gruber S. 2011. Scale-dependent measurement and analysis of ground surface temperature variability in alpine terrain. The Cryosphere 5 : 431-443.

Haeberli W. 1975. Untersuchungen zur Verbreitung von Permafrost zwischen Flüelapass und Piz Grialetsch (Graubünden). Mitteilungen derVAW-ETHZürich 17.

Haeberli W, Hallet B, Arenson L, Elconin R, Humlum O, Kääb A, Kaufmann V, Ladanyi B, Matsuoka N, Springman S, Vonder Mühll D. 2006. Permafrost creep and rock glacier dynamics. Permafrost and Periglacial Processes 17 : 189-214.

Handy MR, Schmid SM, Bousquet R, Kissling E, Bernoulli D. 2010. Reconciling plate-tectonic reconstructions of Alpine Tethys with the geological-geophysical record of spreading and subduction in the Alps. Earth-Science Reviews 102(3-4) : 121-158.

Ilyashuk BP, Ilyashuk EA, Psenner R, Tessadri R, Koinig KA. 2014. Rock glacier outflows may adversely affect lakes: lessons from the past and present of two neighboring water bodies in a crystalline-rock watershed. Environmental Science & Technology 48 : 6192-6200.

Ishido T, Pritchett JW. 1999. Numerical simulation of electrokinetic potentials associated with subsurface fluid flow. Journal of Geophysical Research 104 : 247-259.

Kääb A, Reichmuth T. 2005. Advance mechanisms of rock glaciers. Permafrost and Periglacial Processes 16 : 187-193.

Krainer K, Mostler W. 2002. Hydrology of active rock glaciers: examples from the Austrian Alps. Arctic, Antarctic, and Alpine Research 34 : 142-149.

Krainer K, Mostler W, Spötl C. 2007. Discharge from active rock glaciers, Austrian Alps: A stable isotope approach. Austrian Journal of Earth Sciences 100 : 102-112.

Krainer K, Mussner L, Behm M, Hausmann H. 2012. Multi-disciplinary investigation of an active rock glacier in the Sella Group (Dolomites; Northern Italy). Austrian Journal of Earth Sciences 105(2) : 48-62.

Lachhab A, Booterbaugh A, Beren M. 2014. Bathymetry and sediment accumulation of Walker Lake, PA using two GPR antennas in a new integrated method. Journal of Environmental Engineering Geophysics 20(3) : 245-255.

Langston G, Hayashi M, Roy JW. 2013. Quantifying groundwater-surface water interactions in a proglacial moraine using heat and solute tracers. Water Resources Research 49(9) : 5411-5426.

Loke MH, Lane JW. 2004. Inversion of data from electrical resistivity imaging surveys in water-covered areas. Exploration Geophysics 35(4) : 266-271.

McVey S, Schoeneberger PJ, Turenne J, Payne M, Wysocki DA. 2012. Subaqueous soils (SAS) description. Field Book for Describing and Sampling Soils. National Soil Survey Center Natural Resources Conservation Service U.S. Department of Agriculture.

Millar CI, Westfall RD. 2008. Rock glaciers and related periglacial landforms in the Sierra Nevada, CA, USA: inventory, distribution, and climatic relationships. Quaternary International 188 : 90-104.

Millar CI, Westfall RD, Delany DL. 2013. Thermal and hydrologic attributes of rock glaciers and periglacial talus landforms: Sierra Nevada, California, USA. Quaternary International 310 : 169-180.

Mitchell N, Nyquist JE, Toran L, Rosenberry DO, Mikochik JS. 2008. Electrical resistivity as a tool for identifying geologic heterogeneities which control seepage at Mirror Lake. 21st Symposium on the Application of Geophysics to Engineering and Environmental Problems.

Monteith JL. 1985. Evaporation from land surfaces: progress in analysis and prediction since 1948. Proceedings of the National Conference on Advances in Evapotranspiration 4-12.

Nyquist JE, Freyer PA, Toran L. 2008. Stream bottom resistivity tomography to map ground water discharge. Ground Water 46(4) : 561-569.

Penman HL. 1948. Natural evaporation from open water, bare soil and grass. Proceeding of the Royal Meteorological Society A193 : 120-145.

Potter, N. Jr. 1972. Ice-cored rock glacier, Galena Creek, northern Absaroka Mountains, Wyoming. Geological Society of America Bulletin 83(10) : 3025-3057.

Rangecroft S, Harrison S, Anderson K. 2015. Rock glaciers as water stores in the Bolivian Andes: an assessment of their hydrological importance. Arctic, Antarctic, and Alpine Research 47(1) : 89-98.

Rucker DF, Noonan GE, Greenwood WJ. 2011. Electrical resistivity in support of geological mapping along the Panama Canal. Engineering Geology 117(1-2) : 121-133.

Sambuelli L, Bava S. 2012. Case study: A GPR survey on a morainic lake in northern Italy for bathymetry, water volume and sediment characterization. Journal of Applied Geophysics 81 : 48-56.

Sambuelli L, Colombo N, Giardino M, Godone D. 2015. A Waterborne GPR Survey to Estimate Fine Sediments Volume and Find Optimum Core Location in a Rockglacier Lake. Proceeding of Near Surface Geoscience - 21st European Meeting of Environmental and Engineering Geophysics. DOI: 10.3997/2214-4609.201413826.

Sambuelli L, Comina C, Bava S, Piatti C. 2011. Magnetic, electrical, and GPR waterborne surveys of moraine deposits beneath a lake: A case history from Turin, Italy. Geophysics 76(6) : 213-224.

Schmidt C, Conant Jr B, Bayer-Raich M, Schirmer M. 2007. Evaluation and field-scale application of an analytical method to quantify groundwater discharge using mapped streambed temperatures. Journal of Hydrology 347 : 292-307.

Siegel D. 2008. Reductionist hydrogeology: ten fundamental principles. Hydrological Processes 22 : 4967-4970.

Steck A, Masson H, Robyr M. 2015. Tectonics of the Monte Rosa and surrounding nappes (Switzerland and Italy): Tertiary phases of subduction, thrusting and folding in the Pennine Alps. Swiss Journal of Geosciences 108 : 3-34.

Thies H, Nickus U, Tessadri R, Psenner R. 2007. Unexpected response of high alpine lake Waters to climate warming. Environmental Science & Technology 41 : 7424-7429.

Vaccaneo D, Sambuelli L, Marini P, Tascone R, Orta R. 2004. Measurement system of complex permittivity of ornamental rocks in L frequency band. IEEE transaction on geoscience and remote sensing 42 : 2490-2498.

Vittori Antisari L, Carbone S, Ferronato C, Simoni A, Vianello G. 2011. Characterization of heavy metals atmospheric deposition for assessment of urban environmental quality in the Bologna city (Italy). EQA - International Journal of Environmental Quality 7(7) : 49-63.

Williams MW, Knauf M, Caine N, Liu F, Verplanck PL. 2006. Geochemistry and source waters of rock glacier outflow Colorado Front Range. Permafrost and Periglacial Processes 17 : 13-33.

Rock glacier morphometric characteristics	
Minimum elevation of the front	2706 m a.s.l.
Rooting zone elevation	2816 m a.s.l.
Maximum length	340 m
Maximum width	160 m
Area	37,500 m^2
Maximum height of the front	25 m
Maximum marginal slope	46°
Mean surface slope angle	18°
Pond morphometric characteristics	
Maximum length	60 m
Maximum width	40 m
Perimeter	160 m
Area	1,600 m^2

Table 1 - Rock glacier and pond morphometric characteristics. The main geomorphological characteristics in the watershed were obtained from a digital orthoimage from the year 2012 (source: Ministero dell'Ambiente e della Tutela del Territorio e del Mare - Geoportale Nazionale, http://www.pcn.minambiente.it/GN) and morphometric analyses were performed using ESRI® ArcGISTM v. 10.1 (Spatial Analyst) and a Digital Terrain Model-DTM (cell size: 2 m x 2 m) produced by Regione Autonoma Valle d'Aosta.

Date (2015)	Water profile depths (cm)	Water profile temperatures (°C)
12 July	20	10.2
	100	10.0
	200	9.7
	300	9.3
9 September	20	9.4
	100	9.3
	200	9.0
	300	8.6

Table 2 - Pond water temperature profile on 12 July and 9 September 2015.

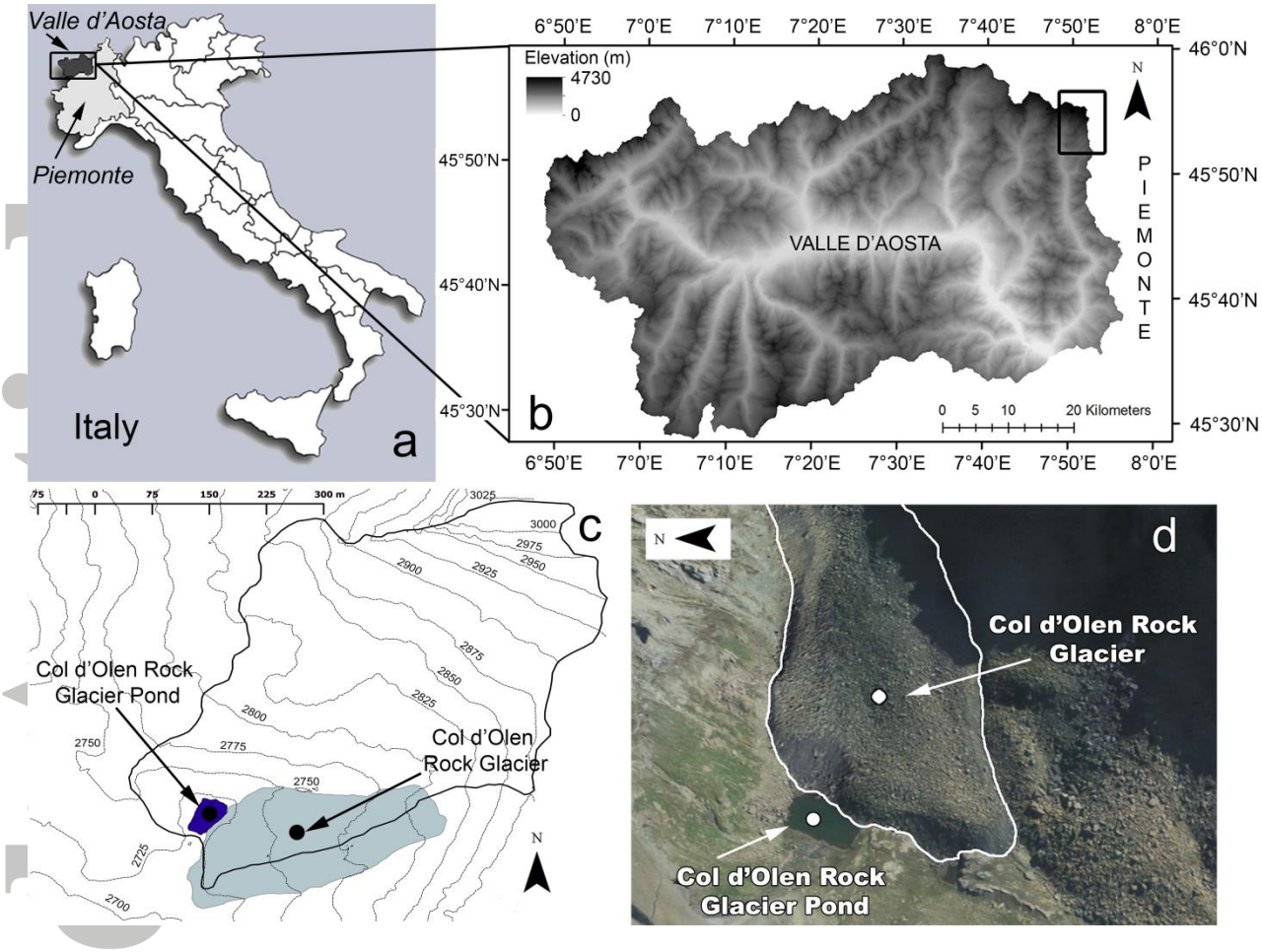

Figure 1 - (a) Location of the study area in Italy. (b) Digital Terrain Model (cell size 10 m x 10 m) of the Valle d'Aosta Region and the location of the study area in the Region. (c) Elevation map (contour line spacing: 25 m) of the Col d'Olen area showing the watershed, the rock glacier, and the pond. (d) Three-dimensional view of the rock glacier and the pond (GeoViewer3D Arpa Piemonte, source: http://webgis.arpa.piemonte.it/geoportale).

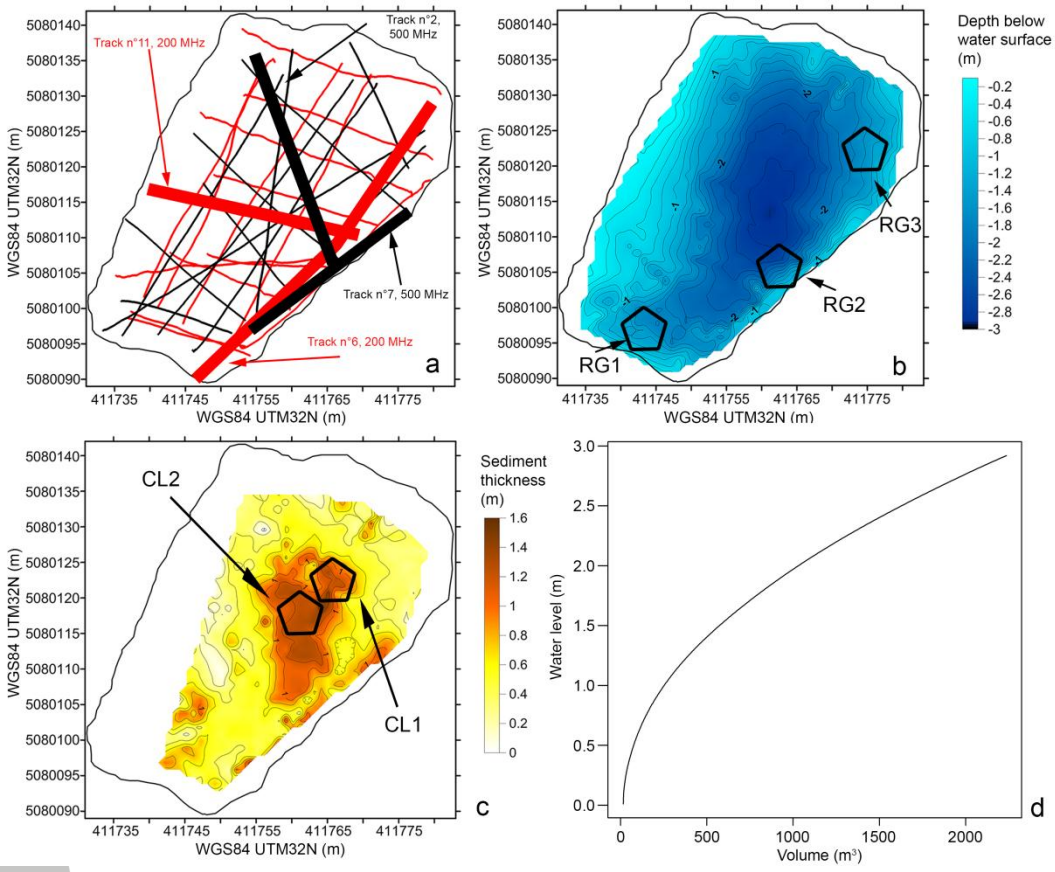

Figure 2 - (a) Tracks of the GPR surveys (red: 200 MHz; black: 500 MHz) and details (thick lines) of the four tracks showed in Fig. 4. (b) Pond bathymetry from the triangular interpolation of the picked bottom reflections from all the radargrams. Black bordered polygons: thermal sensor locations. (c) Fine sediment thickness from the difference between the bottom sediment and the bottom pond pickings. Black bordered polygons: locations of the fine sediment lacustrine core locations. (d) Pond hypsographic curve at 1 cm-steps of water level.

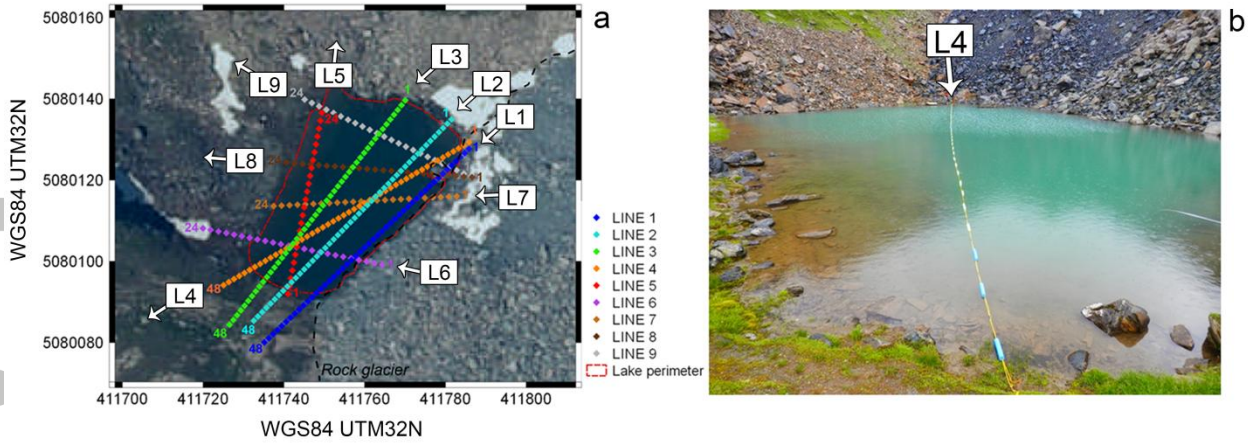

Figure 3 - ERT survey: (a) survey lines (the arrows indicate the line directions) and (b) picture of the floating electrodes (line 4, SW-NE view).

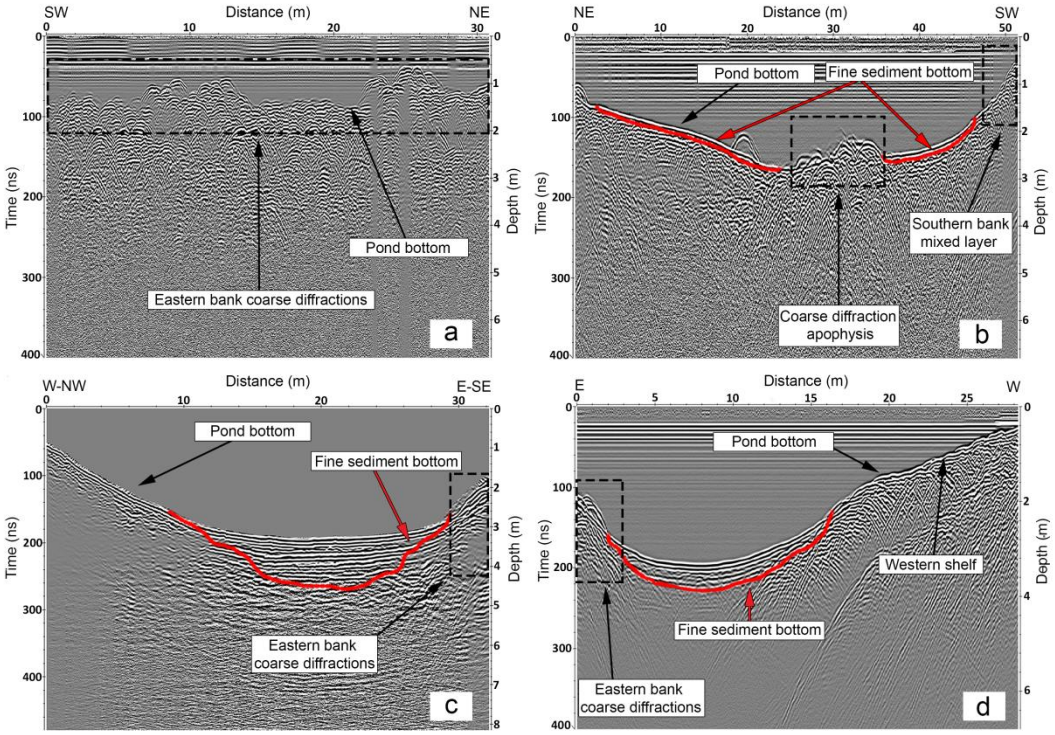

Figure 4 - Pond GPR tracks: (a) track n°7, 500 MHz; (b) track n°6, 200 MHz; (c) track n°2, 500 MHz; (d) track n°11, 200 MHz. The red line in figures a, b and c highlights the limit of the fine-sediment bottom.

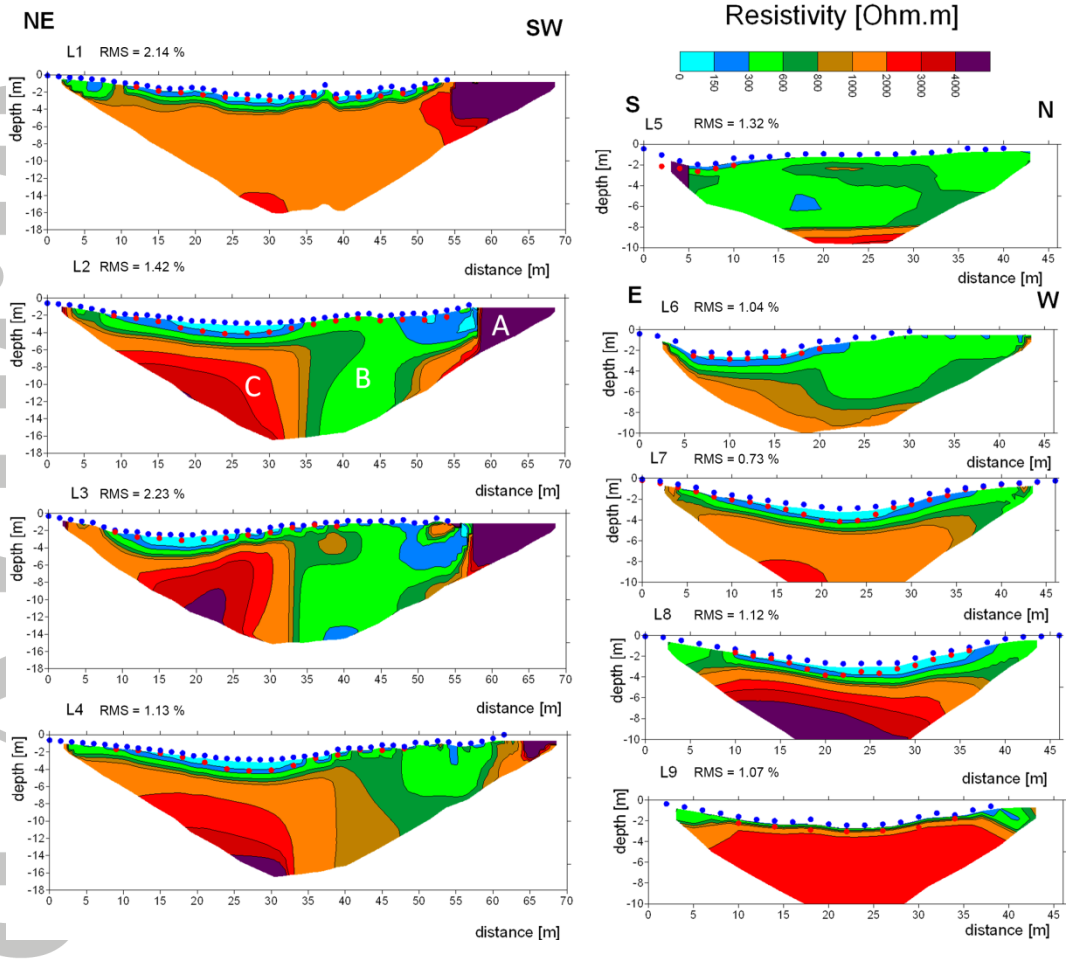

Figure 5 - Interpreted resistivity sections in the pond. For the location of each survey line make reference to Fig. 3a. Blue dotted line: pond bottom from GPR; red dotted line: depth of shallow sediments (second reflector in the GPR). A (massive bedrock), B (low resistivity anomaly) and C (high resistivity body) in L2 highlight the subsurface structures identified in the pond (details in the text). The boundaries of the pond correspond to the presence of bathymetry data.

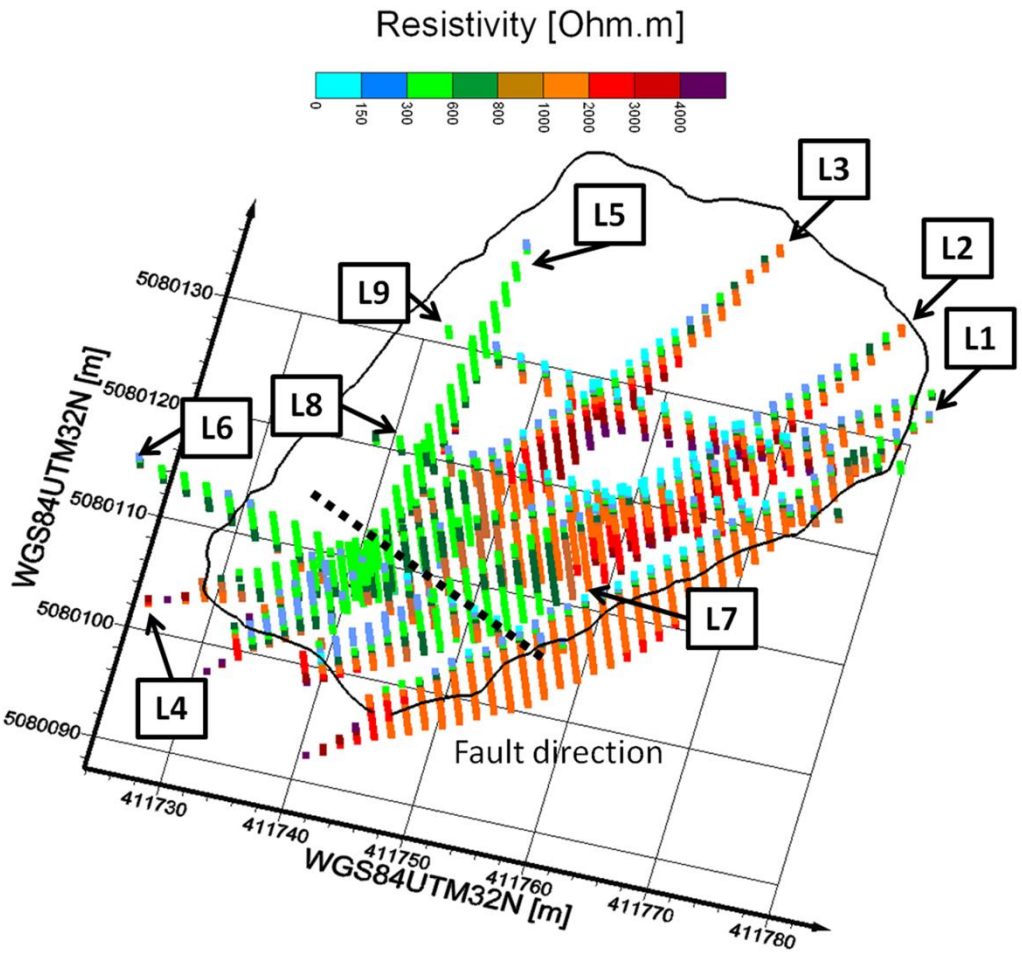

Figure 6 - 3D fence diagram of the ERT inversions with evidence of the survey lines (the arrows indicate the line directions) and of the pond perimeter.

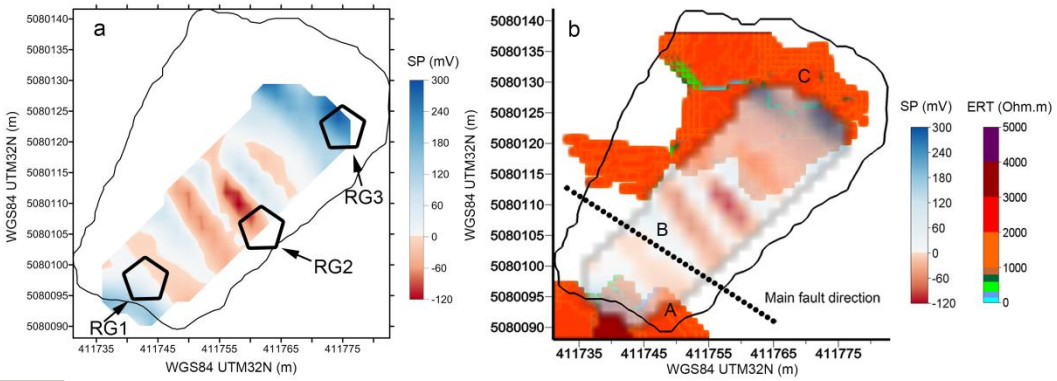

Figure 7 - (a) SP map of survey anomalies (black bordered polygons: thermal sensor locations) and (b) SP map superimposed to the 2000 Ohm•m isosurface from the interpolation of the acquired lines. A (massive bedrock), B (low resistivity anomaly) and C (high resistivity body) (make reference to Fig. 5, L2).

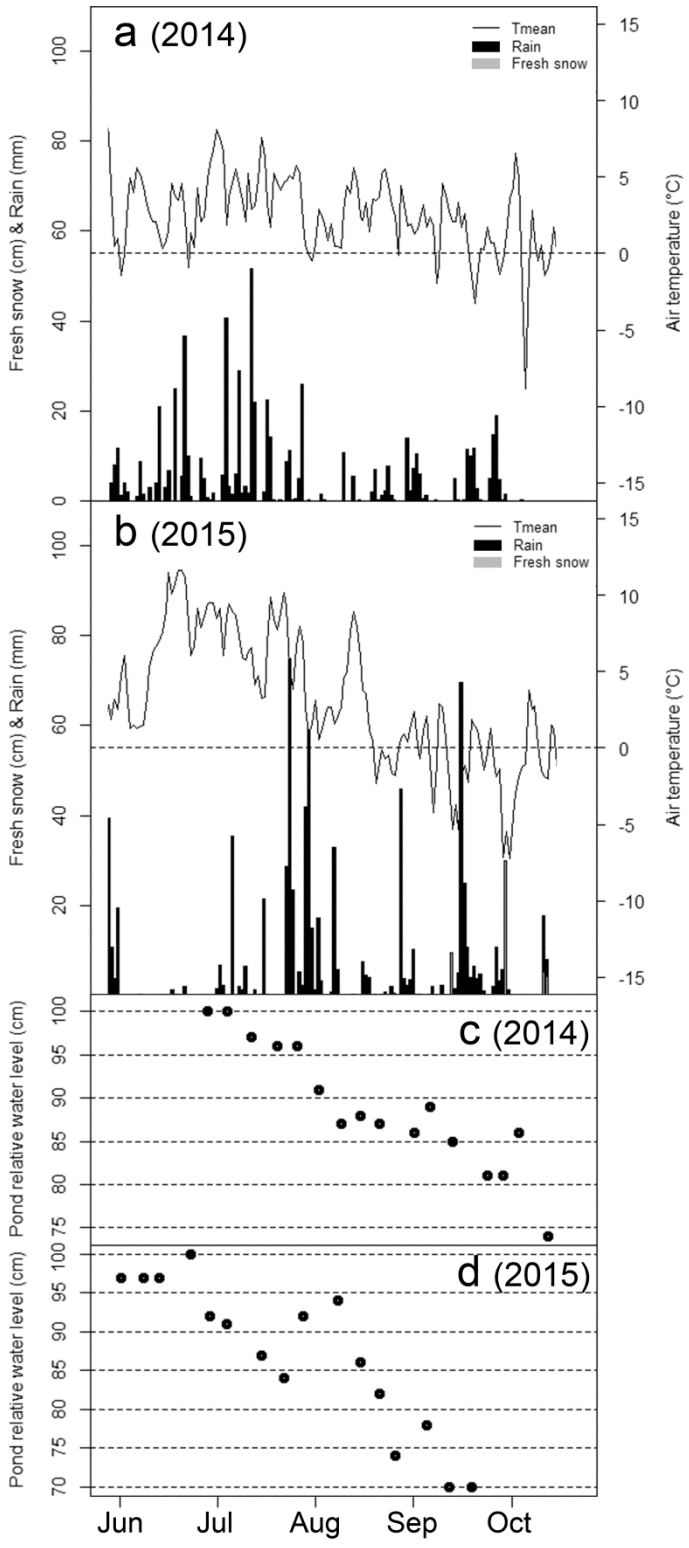

Figure 8 - Precipitation (as fresh snow and rain) and mean daily air temperature for 2014 and 2015 are reported in figures a and b, respectively. Pond relative water level during 2014 (c) and 2015 (d) (hydrometric observations).

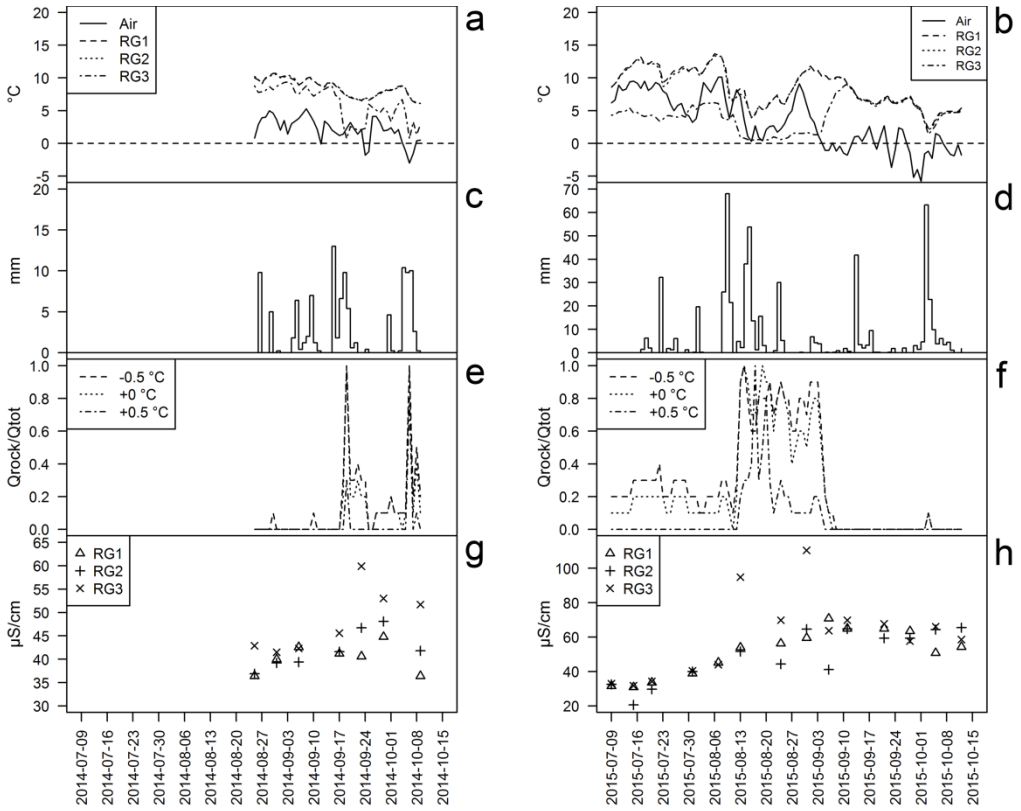

Figure 9 - Air and water temperatures during the investigated periods 2014 (a) and 2015 (b). Precipitation in 2014 (c) and 2015 (d). Rock glacier contribute at RG3 site calculated with the heat tracer approach in 2014 (e) and 2015 (f) assuming meltwater at -0.5, 0, and +0.5 °C. Electrical conductivity in 2014 (g) and 2015 (h).

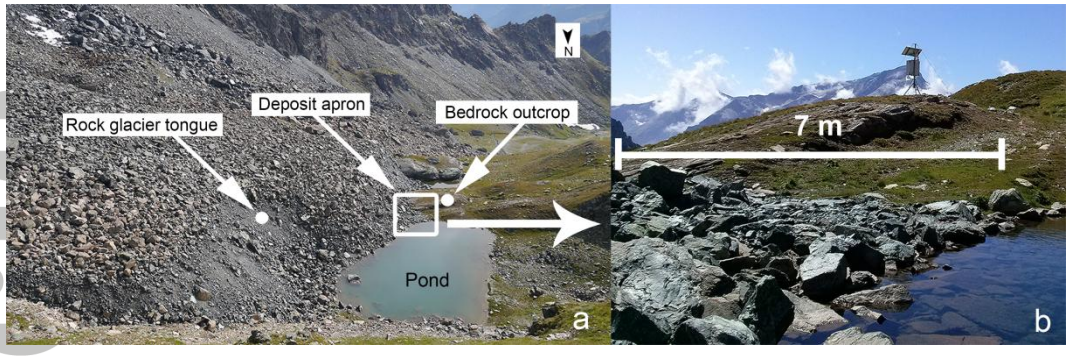

Figure 10 - (a) Picture of the rock glacier tongue flowing into the pond and deposit apron in the southern bedrock outcrop zone; (b) details of the deposit apron.

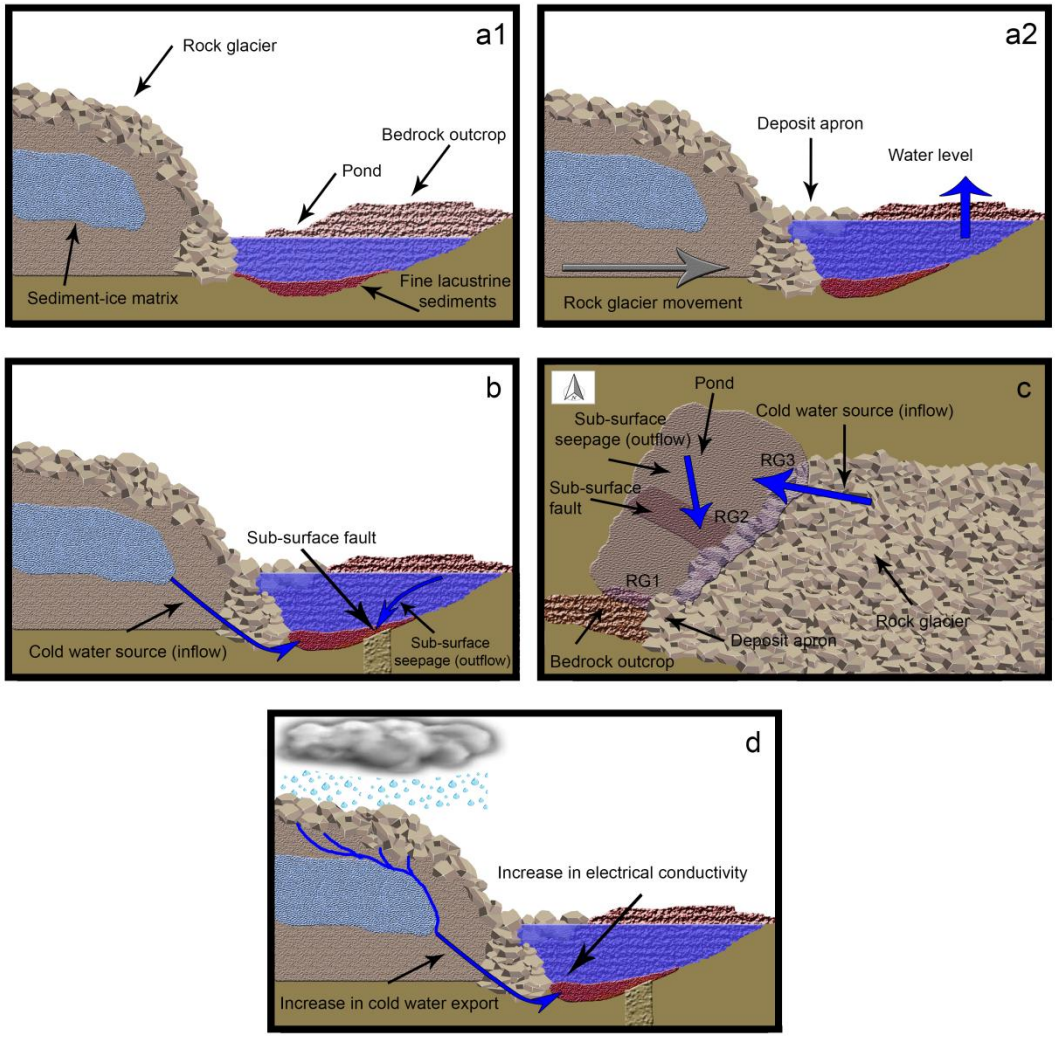

Figure 11 - (a1-a2) Simplified conceptual model of rock glacier advance and progressive filling of the small valley depression. Deposit apron display on southern bedrock outcrop and associated potential modification of water level due to dam formation are also represented. (b) Hydrological dynamics of the rock glacier-pond system (profile representation - b) (planimetric representation - c). (d) Increase in cold water export from the rock glacier after rainfall events, with associated augmentation of electrical conductivity values measured at RG3 site.

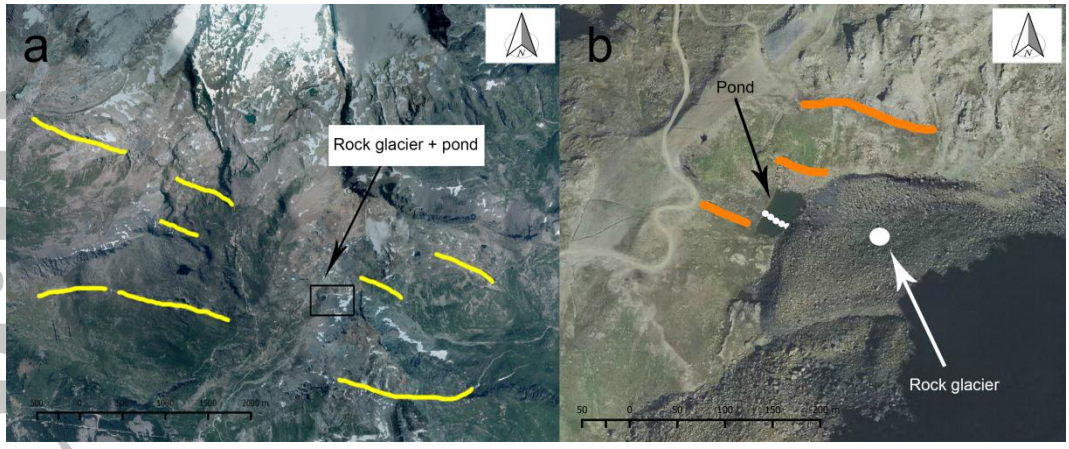

Figure 12 - (a) Large-scale structural evidence in the Col d'Olen area (yellow line: main trench and fault) (digital orthoimage from the year 2012; source: Ministero dell'Ambiente e della Tutela del Territorio e del Mare - Geoportale Nazionale, http://www.pcn.minambiente.it/GN). (b) Fine-scale structural evidence in the rock glacier area (orange line: minor trench and fault; white dotted line: sub-surface minor fault direction) (digital orthoimage from the year 2006; source: Ministero dell'Ambiente e della Tutela del Territorio e del Mare - Geoportale Nazionale, http://www.pcn.minambiente.it/GN). The lower-resolution digital orthoimage 2006 was chosen for showing minor fault directions at fine scale because of the complete absence of snow in the analysed area which partially conceals the structural setting in the higher-resolution digital orthoimage 2012.

Mechanisms linking active rock glaciers and impounded surface water formation in high-mountain areas

Nicola Colombo*, Luigi Sambuelli, Cesare Comina, Chiara Colombero, Marco Giardino, Stephan Gruber, Gaetano Viviano, Livia Vittori Antisari, and Franco Salerno

Rock glacier hydrology and structural setting of a marginal pond are investigated integrating waterborne geophysics and heat tracers. Rock glacier movement has modified the pond structure and water level. A sub-surface hydrological window connects the rock glacier to the pond. Greater water contribution from the landform occurs following intense precipitation, with increasing electrical conductivity values. A sub-surface seepage drives the outflowing dynamic of the pond. The applied approach could be transferred to wider scales of investigation.